JACS
JOURNAL OF THE AMERICAN CHEMICAL SOCIETY
pubs.acs.org/JACS
Article

Cobalt(II)-Substituted Cysteamine Dioxygenase Oxygenation Proceeds through a Cobalt(III)-Superoxo Complex

Jiasong Li,* Ran Duan, and Aimin Liu*

Cite This: J. Am. Chem. Soc. 2024, 146, 18292−18297
Read Online

ABSTRACT: We investigated the metal-substituted catalytic activity of human cysteamine dioxygenase (ADO), an enzyme pivotal in regulating thiol metabolism and contributing to oxygen homeostasis. Our findings demonstrate the catalytic competence of cobalt(II)- and nickel(II)-substituted ADO in cysteamine oxygenation. Notably, Co(II)-ADO exhibited superiority over Ni(II)-ADO despite remaining significantly less active than the natural enzyme. Structural analyses through X-ray crystallography and cobalt K-edge excitation confirmed successful metal substitution with minimal structural perturbations. This provided a robust structural basis, supporting a conserved catalytic mechanism tailored to distinct metal centers. This finding challenges the proposed high-valent ferryl-based mechanism for thiol dioxygenases, suggesting a non-high-valent catalytic pathway in the native enzyme. Further investigation of the cysteamine-bound or a peptide mimic of *N*-terminus RGS5 bound Co(II)-ADO binary complex revealed the metal center's high-spin ($S = 3/2$) state. Upon reaction with O_2, a kinetically and spectroscopically detectable intermediate emerged with a ground spin state of $S = 1/2$. This intermediate exhibits a characteristic ^{59}Co hyperfine splitting ($A = 67$ MHz) structure in the EPR spectrum alongside UV−vis features, consistent with known low-spin Co(III)-superoxo complexes. This observation, unique for protein-bound thiolate-ligated cobalt centers in a protein, unveils the capacities for O_2 activation in such metal environments. These findings provide valuable insights into the non-heme iron-dependent thiol dioxygenase mechanistic landscape, furthering our understanding of thiol metabolism regulation. The exploration of metal-substituted ADO sheds light on the intricate interplay between metal and catalytic activity in this essential enzyme.

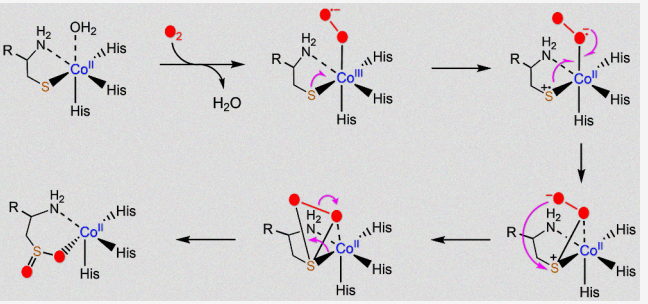

INTRODUCTION

Cysteamine dioxygenase (ADO) plays a pivotal role in regulating mammalian thiol metabolism by oxidizing cysteamine (also known as 2-aminoethanethiol, 2-AET) and, like plant cysteine oxidases (PCO), regulating oxygen homeostasis by targeting *N*-terminal cysteine-containing proteins for oxygen sensing.[1−3] Despite its physiological significance, the catalytic mechanism of ADO remains largely unexplored.

Two proposed mechanistic pathways emerge from the extensive characterization of the founding member of the thiol dioxygenase superfamily, cysteine dioxygenase (CDO), and the synthetic non-heme Fe model complexes.[3−12] O_2, a diradical molecule, ligates to the substrate-bound Fe(II) center, forming an Fe(III)-bound single radical in the form of superoxo, marking the divergence of the two pathways (Scheme 1). The pathway illustrated at the top involves non-ferryl-dependent concurrent dioxygen transfer to the thiolate group of the bound L-cysteine substrate. In this mechanism, thiol and O_2 ligation to the ferrous center results in the free radical character of both substrates, enabling direct radical coupling. Subsequent sulfur addition to the iron-bound proximal oxygen results in the formation of a persulfenate intermediate, and heterolytic O−O cleavage of the following thiadioxirane intermediate

Scheme 1. Proposed ADO Catalytic Pathways[a]

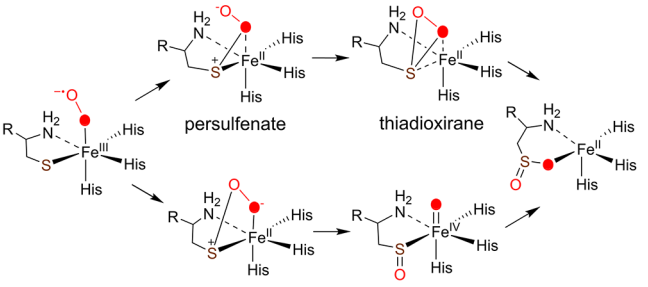

[a]Note that a dashed line does not represent a bond. One ADO substrate, 2-AET, has been proposed to act as a monodentate ligand.

Received: February 5, 2024
Revised: June 12, 2024
Accepted: June 13, 2024
Published: June 28, 2024

https://doi.org/10.1021/jacs.4c01871
J. Am. Chem. Soc. 2024, 146, 18292−18297

yields a sulfinic acid product. This pathway can be facilitated by stabilizing the persulfenate with multiple H-bond interactions from a Cys-Tyr cofactor once it is formed.[4,13−15] The second pathway, analogous to many carbon-targeted oxygenations, follows a traditional oxygen activation mechanism featuring stepwise O atom transfers involving a ferryl species, first distal oxygen and then proximal oxygen. This pathway was proposed based on a computational study, but attempts to trap the ferryl intermediate have been unsuccessful.[10] The key difference between the two mechanistic hypotheses is how the dioxygen forms the first S−O bond with the metal-bound thiol substrate. The first pathway takes advantage of the targeted substrate being an electron-rich thiol, and proximal oxygen transfer leads to the near-simultaneous addition of dioxygen to the thiol before O−O bond cleavage. The stepwise pathway is initiated from distal oxygen transfer, which results in a two-step consecutive monooxygenation process. This pathway involves O−O bond cleavage before completion of O atom transfers and formation of a powerful Fe(IV)=O intermediate capable of oxidizing a wide range of carbon-, nitrogen-, and sulfide-based substrates.

While both pathways are plausible, no consensus has been reached. Experimentally, few catalytic intermediates have been spectroscopically observed in the studies of CDO, and their identity is pending further characterization.[10,16] Interestingly, the anticipated Fe^{2+}-bound persulfenate of the first pathway has been consistently observed in six reported high-resolution crystal structures.[4,17] Notably, the thiol to Fe-bound proximal oxygen is invariant at a distance of 1.7 Å in these structures, consistent with an expected S−O bond between the two substrates. In contrast, the thiol to the distal oxygen from iron is 2.6−3.2 Å (average 2.9 Å in those 1.25−1.63 Å resolution crystal structures, Table S1). The formation of persulfenate is also supported by a computational study and crystal structure of the ternary complex using nitric oxide as an O_2 surrogate, which shows nitrogen, equivalent to proximal oxygen, is closer to the thiol in the ternary complex.[18] However, the mechanism remains highly debatable because a mass spectrometry study shows Fe^{2+}-bound persulfenate occurring only in the crystal and not in the surrounding drop by a different team.[5] ADO crystal structures from human and mouse origins have become available recently.[19,20] Despite significant research efforts, the mechanism by which non-heme iron facilitates thiol oxidation in ADO,[1,15,21,22] and to a large degree CDO, remains an open question for further exploration. ADO and CDO are in the distinct subfamily of proteins within the thiol dioxygenase superfamily[23] and are more closely related to PCO, yet their chemical reaction on the small organic substrate is most similar to that of CDO. These thiol dioxygenases from distinct subfamilies may or may not share the same preference with respect to the mechanistic details in the absence or presence of the cross-linked protein cofactor.

Here, we investigated the thiol oxygenation mechanism using a metal-swapping approach. We generated human ADO (hADO) variants with metal substitutions using transition metal ions and evaluated their catalytic activity. The obtained results offer novel insights into achieving dioxygenation in iron-dependent thiol dioxygenases.

EXPERIMENTAL SECTION

Human ADO expression, isolation, purification, and preparation of near metal-free "apo-ADO" and metal reconstitution procedures are described in the Supporting Information. Briefly, 1,10-phenanthroline and EDTA were used as metal chelators anaerobically. The small molecule substrate cysteamine (98% purity) was purchased from Acros Organics. The RGS5 peptide substrate was synthesized by Biomatik with the sequence of CKGLAALPHSCLER (>95% purity), corresponding to the first 14 amino acids of the Met-excised *N*-terminus of RGS5 as described in a previous report.[21] Catalytic assays were conducted using two independent methods: an oxygen consumption assay using Oxygraph and a product assay using an HPLC-MS method, as described elsewhere.[23] Kinetic analysis was conducted using stopped-flow UV−vis experiments on an Applied Photophysics SX20 spectrophotometer, and data were analyzed using SX Pro-Data Viewer analysis software.

EPR spectroscopic characterization was conducted on a Bruker E560 X-band spectrometer equipped with a cryogen-free 4 K temperature system with an SHQE-W high-Q resonator at 100 kHz modulation frequency which has been described elsewhere.[24,25] Quantitative simulation of the EPR spectra was performed with EasySpin.[26] O_2-free cysteamine or RGS5 peptide was added to the enzyme to the final concentration under anaerobic conditions. An equal volume of O_2-saturated buffer was added to anaerobic Co(II)-ADO with 2-AET or RGS5 before being frozen at various intervals. The samples were transferred to quartz EPR tubes and slowly frozen in liquid ethane or nitrogen for spectroscopic analysis.

Crystallization was conducted using the hanging drop vapor-diffusion method with concentrated Co(II)-ADO (30 mg/mL) in 0.1 M Bis-Tris-HCl (pH 5.5), 0.2 M $(NH_4)_2SO_4$, and 20% (w/v) PEG3350 at 289 K. Fe(II)-ADO crystallization was conducted in an O_2-free anaerobic chamber. Crystals were cryoprotected with crystallization buffer containing an additional 20% (v/v) glycerol and then flash-cooled in liquid nitrogen. Crystallographic data were acquired at Stanford Synchrotron Radiation Lightsource beamline BL 9-2 and the Advanced Photon Sources (Argonne National Laboratory, Argonne, IL) beamline 19BM. Molecular replacement was performed using the crystal structure of Ni(II)-hADO as a starting model (Protein Data Bank entry 7REI).[19]

RESULTS AND DISCUSSION

We assessed the catalytic activity of metal-substituted ADO toward cysteamine and monitored hypotaurine formation in an air-saturated buffer by HPLC-MS, as illustrated in Figure 1A and Figure S1. The nearly metal-free apo-ADO was obtained by treating the protein with iron chelators. We generated metal-substituted human ADO by adding metal ions into "apo-ADO". The metal-stripped ADO proteins contained approximately 1% or less iron ion, resulting in a significant reduction

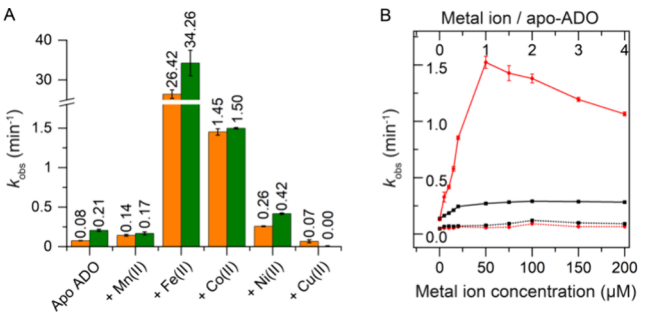

Figure 1. Activity assay of metal-substituted human ADO. (A) Comparison of 2-AET dioxygenation by human ADO in air- (orange) and O_2- (green) saturated buffer by monitoring the product formation using HPLC-MS. (B) Activity assay of metal-stripped ADO (50 μM) with Co(II) (red) or Ni(II) (black) at variable concentrations. The dashed traces show the control group, including only 2-AET and free metal ions.

https://doi.org/10.1021/jacs.4c01871
J. Am. Chem. Soc. 2024, 146, 18292−18297

in catalytic activity compared to the as-isolated Fe(II)-ADO (Figure S2, Table S2).

Notably, Co(II)-ADO and Ni(II)-ADO, generated through metal reconstitution, displayed activity. Co(II)-ADO exhibited k_{obs} of approximately (18.7 ± 0.7)-fold higher than that of "apo-ADO," which contained trace iron, while Ni(II)-ADO showed a (3.3 ± 0.11)-fold increase, albeit these are still a small fraction compared to that of as-isolated Fe(II)-ADO. Mn-ADO displayed slightly higher k_{obs} than that of "apo-ADO" (less than 1.9-fold), while Cu-ADO displayed the lowest one (~0.9-fold). In the O_2-saturated buffer with approximately 1 mM O_2, all samples, except Cu-ADO, exhibited higher activity (Table S3). Additionally, the varied k_{obs} ratio between Co-ADO and Fe-ADO in the O_2 or air-saturated buffers suggests different affinities for the O_2 among these enzymes. Likewise, the as-isolated Co(II)-ADO obtained through a distinct approach also presented substantial activity (Figure S2). In this approach, Co(II)-ADO was synthesized by cells grown in an M9 medium supplemented with $CoCl_2$ and purified by using a cobalt-IMAC resin column.

Subsequently, we incubated the "apo-ADO" protein with varying Co(II) concentrations for activity correlation. As depicted in Figure 1B, the activity continuously increased as the Co(II)/ADO ratio remained below 1.0. However, ADO displayed reduced activity with further increases in the ratio, indicating a metal saturation and possibly protein denaturation induced by excess Co(II) ions at high ratios. Ni(II)-ADO also observed a plateau at a 1:1 ratio.

To directly determine if any structural changes occur as a result of the metal substitution in ADO, especially if Co(II)-ADO and Fe(II)-ADO share a similar metal coordination environment, we determined the crystal structures of Co(II)-ADO and Fe(II)-ADO (Table S4). As illustrated in Figure 2A,

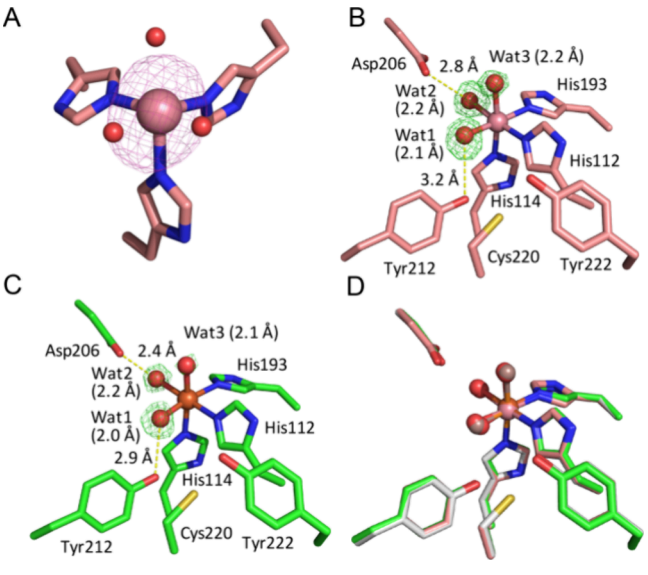

Figure 2. Determination of crystal structures of human ADO. (A) Anomalous difference maps of cobalt in metal-substituted ADO. (B) Active site architecture of Co-ADO. (C) Active site of the Fe(II)-ADO. (D) Superposition of Co-ADO (magenta), Fe-ADO (green), and Ni-ADO (gray) metal centers. The anomalous difference maps, contoured at 6 σ and colored in purple, were calculated from a data set collected at cobalt K-edge (1.605 Å). The $F_o - F_c$ maps, contoured at 6 σ and colored in green, were calculated from data sets collected at selenium K-edge (0.979 Å).

the structure of Co-ADO shows a cobalt ion that is accounted for by the anomalous difference maps. The MAD scans for the crystal indicated the presence of cobalt, and Co K edge excitation scans implied the high occupancy of cobalt in the crystal (Figure S3). The X-ray crystal structure of Co(II)-ADO was determined at a 1.99 Å resolution (Table S4). The Co(II)-coordinated residues in an octahedral coordination environment composed of His97, His112, and His114, and three water molecules occupy the remaining coordination sites (Figure 2B). We have recently reported the first human ADO structure at 1.78 Å resolution with the Fe(II) substituted by a Ni(II) ion.[19] A human ADO structure with an iron ion is needed for a precise comparison to the native enzyme. We then crystallized Fe(II)-ADO synthesized in an M9 minimal medium supplemented with $Fe(NH_4)_2(SO_4)_2$. The crystallization was set up anaerobically. The crystal structure of human Fe(II)-ADO was finally determined at 2.01 Å resolution (Figure 2C).

Hence, these coordinates allowed a direct structural comparison among the native and metal-substituted human ADO variants. The Co(II)-ADO structure closely resembles the Fe(II)-ADO (an RMSD of 0.134 Å for 192 C_α atoms) and Ni(II)-ADO (an RMSD of 0.094 Å for 209 C_α atoms) structures. These structural data demonstrate the preservation of the active site architecture of this human enzyme after metal swapping and an unchanged first and second coordination spheres (Figure 2D). Consequently, the observed metal substitution predominantly influences catalytic activity and has minimal impact on the protein structure. It should be noted that the Cys220-Tyr222 cross-link was not observed due to a missing oxidation step to promote its synthesis. Such a cross-link has previously been observed after processing Fe(II)-ADO with excess 2-AET and O_2, with nearly half of the protein bearing the protein cofactor, even with the added challenge of F_2-Tyr222 substitution.[15]

We conducted spectroscopic characterization of the Co(II)-ADO reaction. Initially, oxygen consumption of 2-AET mediated by Co(II)-ADO was monitored using an oxygen electrode following a previously described protocol.[21] The results depicted in Figure 3A reveal a significantly higher initial rate of O_2 consumption in the presence of Co(II)-ADO compared to "apo-ADO" and its absence (−72 vs −6.0 vs −3.6 μM min^{-1}). The free Co(II) ions do not facilitate 2-AET oxygenation (Figure 1B and Figure S1), although they consume approximately a near-stoichiometric amount of O_2 to form an unproductive complex (Figure 3A) similar to a recently reported thiolate-ligated Co(III)-peroxo complex.[27] This observation supports that Co(II)-ADO consumes O_2 during a multiple turnover catalytic process. The O_2 consumption rate (1.44 min^{-1}) is consistent with the estimated product formation rate of 1.48 min^{-1} (Figure S2). Figure 3B presents the optical spectra of Co(II)-ADO, the binary complex, and the potential ternary complexes. The resting state spectrum exhibited a shoulder beyond 310 nm. Upon anaerobically adding 2-AET, the intensity of the 310 nm shoulder increased slightly, as shown in the difference spectrum. 2-AET-Co(II)-ADO mixed with an O_2-saturated buffer displayed a distinct spectrum, featuring a much stronger peak around 316 nm. This feature aligns with reported Co(III)-superoxo moieties in thiolate-ligated cobalt complexes outside a protein.[28−31] The formation of this ternary complex remained unaffected by catalase or superoxide dismutase (SOD) (Figure S4), indicating it is not a byproduct of a side pathway.

https://doi.org/10.1021/jacs.4c01871
J. Am. Chem. Soc. 2024, 146, 18292−18297

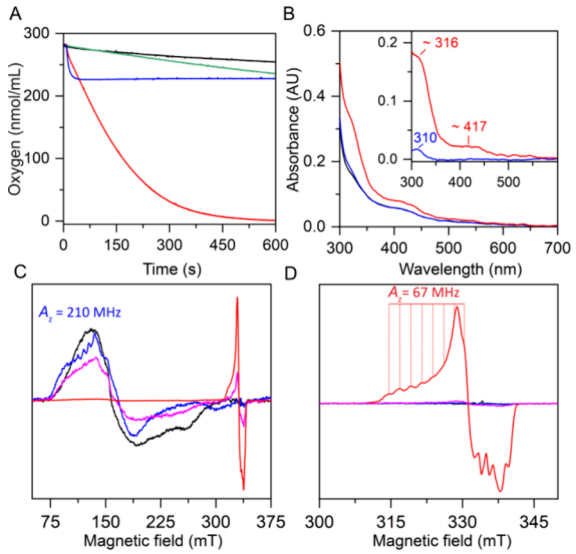

Figure 3. Spectroscopic investigation of the Co-ADO reaction by oxygen electrode, optical, and EPR spectroscopy. (A) Oxygen consumption by 2-AET (black), 2-AET upon adding "apo-ADO" (green), Co(II) ion (blue), or Co(II)-ADO (red). (B) Optical spectra of anaerobic Co(II)-ADO (43.5 μM, black) upon adding 1 mM 2-AET anaerobically (blue) and subsequent addition of O_2-saturated buffer (red). The inset shows difference spectra. (C) EPR of 100 μM Co(II)-ADO (black) and upon addition of 1 mM 2-AET anaerobically (blue) and O_2 for 10 s (red) and 10 min (magenta) (3.17 mW at 30 K). The intensity of the red trace is reduced to 1/10 to match the intensity of the other two traces. (D) Zoom-in scan of the low-spin (S = 1/2) species (0.2 mW at 50 K).

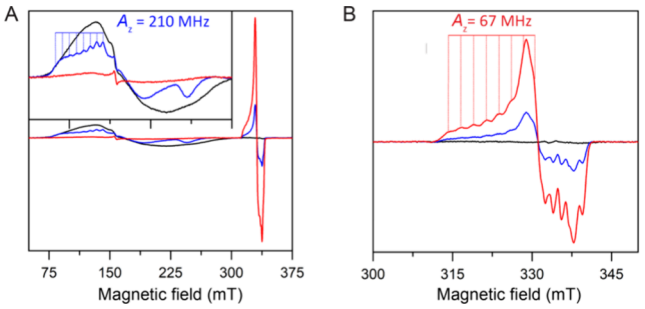

Figure 4. EPR of Co(II)-ADO before (black) and after anaerobic addition of the peptide substrate of the N-terminal sequence of RGS5 (blue) followed by adding O_2 for 10 s (red): (A) full scan range (3.17 mW and 30 K); (B) LS range (0.2 mW and 50 K). The concentrations of Co-ADO and the RGS5 peptide substrate are 200 μM and 5 mM, respectively. The weak LS signal in Co(II)-ADO after adding RGS5 was due to the minute amount of O_2 in the RGS5 stock solution.

As depicted in Figure 3C, substrate-free Co(II)-ADO exhibited a high-spin (HS) center, as we have previously observed from another 3-His ligated Co(II)-substituted center.[32] The EPR spectrum exhibits the characteristics of a typical ground spin state of S = 3/2 Co(II) species with effective g values (g_x, g_y, and g_z) of 2.63, 4.25, and 5.26. Upon anaerobically adding 2-AET, the HS species transformed into a broader rhombic HS signal with g values of 2.25, 4.00, and 5.71, featuring a partially hyperfine structure on g_z. This indicates a coordination state distinct from that of resting Co(II)-ADO and is attributed to the binary complex. Additionally, the Co(II) hyperfine structure on g_z became more apparent when using the N-terminal cysteine-containing RGS5 peptide, displaying eight splitting peaks (A_z = 210 MHz or 7.5 mT) (Figure 4 and Table S5). RGS5 plays a role as a hypoxia-responsive protein that suppresses chemokinetic and chemotactic migration in brain pericytes, which has been shown to be one of the ADO substrates and regulated by ADO's dioxygenase activity.[2,3] A peptide of the first 14 amino acids of the Met-excised N-terminus of RGS5 has been used to mimic RGS5 in the human ADO-substrate interaction studies.[21]

Remarkably, adding an O_2-saturated buffer to anaerobic Co(II)-ADO with 2-AET induced a complete decay of the HS species, revealing a new low spin (LS, S = 1/2) species with g ≈ 2.02 and well-resolved eight splitting hyperfine lines (A_z = 67 MHz or 2.4 mT) attributable to ^{59}Co (Figure 3D), indicating the formation of a ternary complex involving ADO, 2-AET, and O_2. Likewise, Co(II)-ADO with RGS5 also produced the identical LS species after the addition of O_2 (Figure 4). The LS signal follows Curie law behavior up to 50 K, indicating that it does not originate from a spin-coupled signal (Figure S5 and Table S6). The best fit of the data was achieved by considering a single LS species (Figure S6 and Table S7). The features of the LS species align with reported Co(III)-superoxo species in thiolate-ligated cobalt complex[29,30,33] and are comparable with the LS Co(III)-superoxo species reported in Co-substituted extradiol dioxygenase HPCD.[34] These results indicate that Co-ADO can form a ternary complex with 2-AET and O_2. After 10 min, the LS species almost disappeared and the HS species returned to around two-thirds of the initial intensity, suggesting the accumulation of an EPR silent species with a 417 nm broader feature during the reaction under such conditions.

Next, we explored the Co(II)-ADO mediated oxygenation using stopped-flow optical spectroscopy using "apo-ADO" as one of the controls (Figure S7). When anaerobic Co(II)-ADO with 2-AET in a 1:33 ratio was mixed with O_2 and monitored by optical spectroscopy (Figure 5), the ternary complex, indicated by a peak at 316 nm, initially increased dramatically in the millisecond time domain, reaching its maximum within 2 s, then slowly decayed over approximately 1000 s. The corresponding substantial EPR spectral difference suggests that Co-ADO cannot fully revert to the resting state under these conditions after multiple turnovers (Figure S8), aligning with the observation in Figure 3C. On the contrary, apo-ADO did not exhibit the spectral changes (Figure S7). We then executed an approximate "single-turnover" experiment upon mixing O_2-free Co(II)-ADO and 2-AET at a 2:1 ratio, then with O_2. The results shown in Figure S9 and Figure S10 indicate that the kinetics of LS species observed in EPR experiments and 316 nm species observed in stopped-flow experiments are consistent with each other. It is worth noting that the rates of O_2 consumption, taurine formation, and ternary complex decay in these preliminary kinetic explorations are aligned approximately with one another, despite experimental challenges.

It is worth noting that two possible adverse effects of metal substitution can result in less effective catalysis. First, Co(II) has a lower oxygen binding affinity than Fe(II), and this difference could affect O_2 binding, as shown in a metal substitution study of an extradiol dioxygenase.[34,35] Second, the difference in redox potential between Co(II/III) and Fe(II/III) redox couples may contribute to the slower substrate

https://doi.org/10.1021/jacs.4c01871
J. Am. Chem. Soc. 2024, 146, 18292−18297

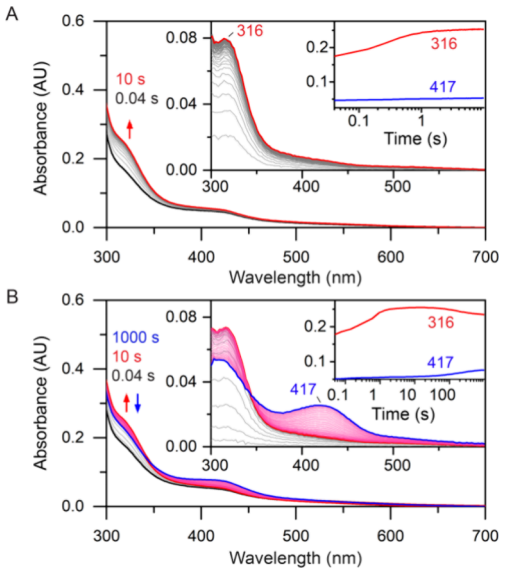

Figure 5. Catalytic assay for Co(II)-ADO and 2-AET reacting with dioxygen. (A, B) Optical spectral changes of anaerobic 30 μM Co-ADO with 1 mM 2-AET upon adding an O_2-saturated buffer. The insets show the difference spectra, and the second layer of insets shows the time traces of absorption intensity at 316, 417, and 351 nm, respectively. The spectrum of Co(II)-ADO at resting state is in black, and spectral changes of 0.04, 10, and 1000 s are in black, red, and blue in panels A and B. Spectral changes from 10 to 1000 s in panel B are marked in magenta, while others are labeled in gray.

oxidation phase after forming the ternary complex, as indicated by its estimated $t_{1/2}$ value (24 s). The cobalt center could enjoy high crystal field stabilization energy at the +3 oxidation state at certain geometries, and the spin transition may also affect the kinetic steps of the reaction. During multiple turnover conditions, the slower substrate oxidation by the putative Co(III)-superoxide may trigger a nonproductive side route and impact the enzyme's ability to fully return to the resting state, as minor EPR-silent Co(III) species were observed after such a reaction (Figures 3C and S7). It should be noted that the Co(II)-substitution in other none-heme Fe-dependent dioxygenases either supports the reaction (HPCD,[30,31] QueD[27]) or results in catalytically inert protein variants (DMO[36] and TauD[37]).

CONCLUSION

In summary, the results of this study confirmed the catalytic activity of Co(II)-ADO on 2-AET for dioxygenation using an HPLC-MS-based assay. The X-ray crystallographic study suggested metal substitution with Co(II) and Ni(II) mainly affected catalytic activity and not protein structure. Optical and EPR spectroscopy of the binary using 2-AET and a peptide mimic of the *N*-terminus of RGS5 revealed a high-spin Co(II) complex. Adding O_2 to the binary complex resulted in a transient ternary complex with spectroscopic characteristics consistent with a low-spin Co(III)-superoxo complex. This study provides valuable insights into the catalytic mechanism of human ADO. Since no mononuclear Co(IV) without a macrocyclic ligand set has been reported in aqueous environments thus far from a biological system or a synthetic complex, the results favor the non-high-valent mechanistic proposal in ADO (Scheme 1, top route), which leads to a concerted dioxygen transfer to the electron-rich thiol group of the substrate.

ASSOCIATED CONTENT

Supporting Information

The Supporting Information is available free of charge at https://pubs.acs.org/doi/10.1021/jacs.4c01871.

Additional experimental details, Tables S1−S7, and Figures S1−S10 (PDF)

Accession Codes

The structural coordinates resulting from this work have been deposited to the PDB with entries 8UAN and 8U9J.

AUTHOR INFORMATION

Corresponding Authors

Jiasong Li − *Department of Chemistry, University of Texas at San Antonio, San Antonio, Texas 78249, United States;* orcid.org/0000-0003-0341-2038; Email: Jiasong.li@utsa.edu

Aimin Liu − *Department of Chemistry, University of Texas at San Antonio, San Antonio, Texas 78249, United States;* orcid.org/0000-0002-4182-8176; Email: Feradical@utsa.edu

Author

Ran Duan − *Department of Chemistry, University of Texas at San Antonio, San Antonio, Texas 78249, United States;* orcid.org/0000-0002-5370-5990

Complete contact information is available at: https://pubs.acs.org/10.1021/jacs.4c01871

Notes

The authors declare no competing financial interest.

ACKNOWLEDGMENTS

This work was supported by NSF Award CHE-2204225 and partially by using the HPLC equipment from an administrative supplement of NIH Grant R01GM108988. A.L. acknowledges the additional support of Welch Foundation Grant AX-2110-20220331 and Lutcher Brown's endowment. We thank the staff scientists for assisting with remote data collections at beamline 9-2 of the Stanford Synchrotron Radiation Lightsource (SSRL) and beamline 19-BM at the Argonne National Laboratory of Advanced Photon Source (APS). The general user programs of the SSRL and APS are supported by the U.S. Department of Energy (DOE), Office of Science, Office of Basic Energy Sciences under Contracts DE-AC02-76SF00515 and DE-AC02-06CH11357, respectively. The SSRL Structural Molecular Biology Program is supported by the DOE Office of Biological and Environmental Research and NIH Grant P41GM103393.

REFERENCES

(1) Dominy, J. E., Jr; Simmons, C. R.; Hirschberger, L. L.; Hwang, J.; Coloso, R. M.; Stipanuk, M. H. Discovery and characterization of a second mammalian thiol dioxygenase, cysteamine dioxygenase. *J. Biol. Chem.* **2007**, *282*, 25189−25198.

(2) Masson, N.; Keeley, T. P.; Giuntoli, B.; White, M. D.; Puerta, M. L.; Perata, P.; Hopkinson, R. J.; Flashman, E.; Licausi, F.; Ratcliffe, P. J. Conserved *N*-terminal cysteine dioxygenases transduce responses to hypoxia in animals and plants. *Science* **2019**, *365*, 65−69.

(3) Gunawardana, D. M.; Heathcote, K. C.; Flashman, E. Emerging roles for thiol dioxygenases as oxygen sensors. *FEBS J.* **2022**, *289*, 5426−5439.
(4) Simmons, C. R.; Krishnamoorthy, K.; Granett, S. L.; Schuller, D. J.; Dominy, J. E., Jr; Begley, T. P.; Stipanuk, M. H.; Karplus, P. A. A putative Fe^{2+}-bound persulfenate intermediate in cysteine dioxygenase. *Biochemistry* **2008**, *47*, 11390−11392.
(5) Li, J.; Koto, T.; Davis, I.; Liu, A. Probing the Cys-Tyr cofactor biogenesis in cysteine dioxygenase by the genetic incorporation of fluorotyrosine. *Biochemistry* **2019**, *58*, 2218−2227.
(6) Traore, E. S.; Liu, A. Charge maintenance during catalysis in nonheme iron oxygenases. *ACS Catal.* **2022**, *12*, 6191−6208.
(7) Pierce, B. S.; Schmittou, A. N.; York, N. J.; Madigan, R. P.; Nino, P. F.; Foss, F. W.; Lockart, M. M. Improved resolution of 3-mercaptopropionate dioxygenase active site provided by ENDOR spectroscopy offers insight into catalytic mechanism. *J. Biol. Chem.* **2024**, *300*, 105777.
(8) Miller, J. R.; Brunold, T. C. Spectroscopic analysis of the mammalian enzyme cysteine dioxygenase. *Meth. Enzymol.* **2023**, *682*, 101−135.
(9) Aloi, S.; Davies, C. G.; Karplus, P. A.; Wilbanks, S. M.; Jameson, G. N. L. Substrate specificity in thiol dioxygenases. *Biochemistry* **2019**, *58*, 2398−2407.
(10) Tchesnokov, E. P.; Faponle, A. S.; Davies, C. G.; Quesne, M. G.; Turner, R.; Fellner, M.; Souness, R. J.; Wilbanks, S. M.; de Visser, S. P.; Jameson, G. N. An iron-oxygen intermediate formed during the catalytic cycle of cysteine dioxygenase. *Chem. Commun.* **2016**, *52*, 8814−8817.
(11) Tchesnokov, E. P.; Wilbanks, S. M.; Jameson, G. N. A strongly bound high-spin iron(II) coordinates cysteine and homocysteine in cysteine dioxygenase. *Biochemistry* **2012**, *51*, 257−264.
(12) Yadav, S.; Yadav, V.; Siegler, M. A.; Moënne-Loccoz, P.; Jameson, G. N. L.; Goldberg, D. P. A nonheme iron(III) superoxide complex leads to sulfur oxygenation. *J. Am. Chem. Soc.* **2024**, *146*, 7915−7921.
(13) McCoy, J. G.; Bailey, L. J.; Bitto, E.; Bingman, C. A.; Aceti, D. J.; Fox, B. G.; Phillips, G. N., Jr Structure and mechanism of mouse cysteine dioxygenase. *Proc. Natl. Acad. Sci. U.S.A.* **2006**, *103*, 3084−3089.
(14) Li, J.; Griffith, W. P.; Davis, I.; Shin, I.; Wang, J.; Li, F.; Wang, Y.; Wherritt, D. J.; Liu, A. Cleavage of a carbon-fluorine bond by an engineered cysteine dioxygenase. *Nat. Chem. Biol.* **2018**, *14*, 853−860.
(15) Wang, Y.; Griffith, W. P.; Li, J.; Koto, T.; Wherritt, D. J.; Fritz, E.; Liu, A. Cofactor biogenesis in cysteamine dioxygenase: C-F bond cleavage with genetically incorporated unnatural tyrosine. *Angew. Chem., Int. Ed.* **2018**, *57*, 8149−8153.
(16) Crawford, J. A.; Li, W.; Pierce, B. S. Single turnover of substrate-bound ferric cysteine dioxygenase with superoxide anion: enzymatic reactivation, product formation, and a transient intermediate. *Biochemistry* **2011**, *50*, 10241−10253.
(17) Driggers, C. M.; Cooley, R. B.; Sankaran, B.; Hirschberger, L. L.; Stipanuk, M. H.; Karplus, P. A. Cysteine dioxygenase structures from pH 4 to 9: consistent cys-persulfenate formation at intermediate pH and a Cys-bound enzyme at higher pH. *J. Mol. Biol.* **2013**, *425*, 3121−3136.
(18) Souness, R. J.; Kleffmann, T.; Tchesnokov, E. P.; Wilbanks, S. M.; Jameson, G. B.; Jameson, G. N. Mechanistic implications of persulfenate and persulfide binding in the active site of cysteine dioxygenase. *Biochemtry* **2013**, *52*, 7606−7617.
(19) Wang, Y.; Shin, I.; Li, J.; Liu, A. Crystal structure of human cysteamine dioxygenase provides a structural rationale for its function as an oxygen sensor. *J. Biol. Chem.* **2021**, *297*, 101176.
(20) Fernandez, R. L.; Elmendorf, L. D.; Smith, R. W.; Bingman, C. A.; Fox, B. G.; Brunold, T. C. The crystal structure of cysteamine dioxygenase reveals the origin of the large substrate scope of this vital mammalian enzyme. *Biochemistry* **2021**, *60*, 3728−3737.
(21) Wang, Y.; Davis, I.; Chan, Y.; Naik, S. G.; Griffith, W. P.; Liu, A. Characterization of the nonheme iron center of cysteamine dioxygenase and its interaction with substrates. *J. Biol. Chem.* **2020**, *295*, 11789−11802.
(22) Fernandez, R. L.; Dillon, S. L.; Stipanuk, M. H.; Fox, B. G.; Brunold, T. C. Spectroscopic investigation of cysteamine dioxygenase. *Biochemistry* **2020**, *59*, 2450−2458.
(23) Duan, R.; Li, J.; Liu, A. Unveiling the mechanism of cysteamine dioxygenase: A combined HPLC-MS assay and metal-substitution approach. *Methods Enzymol.* **2024**, DOI: 10.1016/bs.mie.2024.05.018.
(24) Fielding, A. J.; Dornevil, K.; Ma, L.; Davis, I.; Liu, A. Probing ligand exchange in the P450 enzyme CYP121 from *Mycobacterium tuberculosis*: Dynamic equilibrium of the distal heme ligand as a function of pH and temperature. *J. Am. Chem. Soc.* **2017**, *139*, 17484−17499.
(25) Dornevil, K.; Davis, I.; Fielding, A. J.; Terrell, J. R.; Ma, L.; Liu, A. Cross-linking of dicyclotyrosine by the cytochrome P450 enzyme CYP121 from *Mycobacterium tuberculosis* proceeds through a catalytic shunt pathway. *J. Biol. Chem.* **2017**, *292*, 13645−13657.
(26) Stoll, S.; Schweiger, A. EasySpin, a comprehensive software package for spectral simulation and analysis in EPR. *J. Magn. Reson.* **2006**, *178*, 42−55.
(27) Li, Y.; Handunnetthige, S.; He, W.; Talipov, M. R.; Wang, D. A Co(III)-peroxo-arylboronate complex formed by nucleophilic reaction of a Co(III)-peroxo species. *J. Inorg. Biochem.* **2024**, *256*, 112552.
(28) Wang, C. C.; Chang, H. C.; Lai, Y. C.; Fang, H.; Li, C. C.; Hsu, H. K.; Li, Z. Y.; Lin, T. S.; Kuo, T. S.; Neese, F.; Ye, S.; Chiang, Y. W.; Tsai, M. L.; Liaw, W. F.; Lee, W. Z. A structurally characterized nonheme cobalt-hydroperoxo complex derived from its superoxo intermediate via hydrogen atom abstraction. *J. Am. Chem. Soc.* **2016**, *138*, 14186−14189.
(29) Fischer, A. A.; Lindeman, S. V.; Fiedler, A. T. Spectroscopic and computational studies of reversible O_2 binding by a cobalt complex of relevance to cysteine dioxygenase. *Dalton Trans.* **2017**, *46*, 13229−13241.
(30) Gordon, J. B.; Vilbert, A. C.; Siegler, M. A.; Lancaster, K. M.; Moenne-Loccoz, P.; Goldberg, D. P. A nonheme thiolate-ligated cobalt superoxo complex: synthesis and spectroscopic characterization, computational studies, and hydrogen atom abstraction reactivity. *J. Am. Chem. Soc.* **2019**, *141*, 3641−3653.
(31) Battistella, B.; Iffland-Muhlhaus, L.; Schutze, M.; Cula, B.; Kuhlmann, U.; Dau, H.; Hildebrandt, P.; Lohmiller, T.; Mebs, S.; Apfel, U. P.; Ray, K. Evidence of sulfur non-innocence in $[Co^{II}(dithiacyclam)]^{2+}$-mediated catalytic oxygen reduction reactions. *Angew. Chem., Int. Ed* **2023**, *62*, No. e202214074.
(32) Li, T.; Walker, A. L.; Iwaki, H.; Hasegawa, Y.; Liu, A. Kinetic and spectroscopic characterization of ACMSD from *Pseudomonas fluorescens* reveals a pentacoordinate mononuclear metallocofactor. *J. Am. Chem. Soc.* **2005**, *127*, 12282−12290.
(33) Muller, L.; Hoof, S.; Keck, M.; Herwig, C.; Limberg, C. Enhancing tris(pyrazolyl)borate-based models of cysteine/cysteamine dioxygenases through steric effects: Increased reactivities, full product characterization and hints to initial superoxide formation. *Chemistry* **2020**, *26*, 11851−11861.
(34) Fielding, A. J.; Lipscomb, J. D.; Que, L., Jr Characterization of an O_2 adduct of an active cobalt-substituted extradiol-cleaving catechol dioxygenase. *J. Am. Chem. Soc.* **2012**, *134*, 796−799.
(35) Fielding, A. J.; Kovaleva, E. G.; Farquhar, E. R.; Lipscomb, J. D.; Que, L., Jr A hyperactive cobalt-substituted extradiol-cleaving catechol dioxygenase. *J. Biol. Inorg. Chem.* **2011**, *16*, 341−355.
(36) D'Ordine, R. L.; Rydel, T. J.; Storek, M. J.; Sturman, E. J.; Moshiri, F.; Bartlett, R. K.; Brown, G. R.; Eilers, R. J.; Dart, C.; Qi, Y.; Flasinski, S.; Franklin, S. J. Dicamba monooxygenase: structural insights into a dynamic Rieske oxygenase that catalyzes an exocyclic monooxygenation. *J. Mol. Biol.* **2009**, *392*, 481−497.
(37) Kalliri, E.; Grzyska, P. K.; Hausinger, R. P. Kinetic and spectroscopic investigation of Co^{II}, Ni^{II}, and *N*-oxalylglycine inhibition of the Fe^{II}/α-ketoglutarate dioxygenase, TauD. *Biochem. Biophys. Res. Commun.* **2005**, *338*, 191−197.

Supporting Information

Cobalt(II)-Substituted Cysteamine Dioxygenase Oxygenation Proceeds Through a Cobalt(III)-Superoxo Complex

Jiasong Li,* Ran Duan, and Aimin Liu*

Department of Chemistry, University of Texas at San Antonio, San Antonio, TX 78249, United States

https://doi.org/10.1021/jacs.4c01871

Table of Content

DETAILED MATERIALS AND EXPERIMENTAL PROCEDURES

MATERIALS

Cysteamine (98% purity) was purchased from Acros Organics. A peptide substrate with a sequence of CKGLAALPHSCLER (>95%) was synthesized by Biomatik, which corresponded to the first 14 amino acids of the Met-excised *N*-terminus of RGS5. Ferrozine, Hypotaurine, HFBA, PEG, metal salts, EDTA, and 1,10-phenanthroline were purchased from Sigma-Aldrich or Thermo Fisher Scientific with the reagent grade or better and used as received. DNA manipulations in *Escherichia coli* were carried out according to standard procedures. Kanamycin (50 μg/mL) was used as antibiotic to select recombinant strains.

BACTERIAL STRAIN AND PLASMIDS

Wild-type (WT) human ADO (hADO) and C18S/C239S hADO variant were cloned to a pET-28a plasmid with a tag-cleavable site containing 30 additional amino acids, including a His_6-tag at *N*-terminus has been described in our previous work.[1] The plasmids were transformed in BL21 (DE3) (Merck).

METHODS AND PROCEDURES

PROTEIN PURIFICATION AND CHARACTERIZATION

The procedures of expression and purification of hADO have been described previously.[1] Cell culture was prepared at 37 °C in an M9 minimal medium within a baffled flask at 220 rpm until OD_{600} reached 0.8 AU. At that time, a supplement of $CoCl_2$ or $Fe(NH_4)_2SO_4$ (20 μM) and isopropyl-β-D-thiogalactopyranoside (IPTG) (0.5 mM) was added. Afterward, the cell culture was continued for 4-6 h before harvesting. The cells were resuspended in the lysis buffer, i.e., 50 mM Tris-HCl and 200 mM NaCl at pH 8.0, and then disrupted by a Microfluidizer LM20 cell disruptor. The supernatant was recovered after centrifugation (34,000g for 40 min) at 4 °C. Intended Fe-ADO protein was purified using Ni-NTA agarose beads, while Co-NTA agarose beads were used for ADO purification intended for Co(II)-reconstitution. After washing the column with washing buffers (50 mM Tris-HCl, 200 mM NaCl, and 10 mM imidazole, pH 8.0), the protein was eluted with elution buffer (50 mM Tris-HCl, 200 mM NaCl, and 300 mM imidazole, pH 8.0). The *N*-terminal His_6-tagged Fe-ADO was mixed with TEV protease and dialyzed into the dialysis buffer (10 mM Tris, 5% glycerol, pH 8.0) overnight. The His_6-tag and uncut protein were removed using IMAC column. The non-tagged hADO proteins were further purified by Superdex 75 (Cytiva) gel-filtration column (16/600) in 50 mM, 50 mM NaCl, pH 7.6 buffer. The purified proteins were either ultra-filtrated to the required concentration for subsequent experiments or stored in 50 mM Tris, 50 mM NaCl, 5% glycerol, pH 7.6 buffer at −80 °C. The protein concentration was determined based on the extinction coefficient of $\varepsilon_{280\ nm}$ = 22,920 $cm^{-1}M^{-1}$. The purity of the protein samples was verified by SDS-PAGE.

PREPARATION OF NEAR METAL-FREE "APO-ADO" AND METAL RECONSTITUTION

The metal-depleted "apo-ADO" was prepared following the previously described method.[2] 200 μM WT ADO was dissolved in the buffer of 50 mM HEPES at pH 8.0 and incubated with 2 mM sodium dithionite, 5 mM 1,10-phenanthroline, and 5 mM EDTA under anaerobic conditions for 1 h. During this period, the solution turned orange-red (λ_{max} = 511 nm), indicating the formation of $[Fe(phen)_3]^{2+}$. The solution was then passed through the desalting column (Bio-Rad) and eluted with HEPES buffer to remove $[Fe(phen)_3]^{2+}$. The obtained protein fraction was concentrated and treated with 2 mM sodium dithionite, 5 mM 1,10-phenanthroline, and 5 mM EDTA, then passed through the desalting column for another two times. We used a ferrozine assay described previously[3-4] and determined the iron content in the "apo-ADO", which was in agreement with the previous ICP-OES-determined iron content of mouse ADO using a similar metal-depleting method.[5]

The metal reconstitution reactions were conducted with the near metal-free "apo-ADO" preparations, which were mixed with the intended metal ions in HEPES buffer at 4 °C for 20 min. The reconstituted protein was used immediately in the HPLC-MS assay described below.

HPLC-MS ASSAY FOR DIOXYGENASE PRODUCT DETECTION

The reaction mixture underwent ultrafiltration using a 10 kDa MWCO ultra centrifugal filter, and the flow-through liquid was separated using an ODS-3 HPLC Column, 3 μm, 100 x 4.6 mm; isocratic elution with a buffer composed of 99.1% H_2O, 0.6% methanol, and 0.3% heptafluorobutyric acid (HFBA) over 10 min at 1.5 mL/min; UV-vis absorbance at 219 nm was monitored. The peak area of the ADO reaction product, hypotaurine, was integrated and fitted to a standard curve to determine its concentration. All experiments were conducted in triplicate. For the Fe-ADO reaction, the system comprised 5 μM "apo-ADO," 5 μM metal ions, and 10 mM cysteamine in a 50 mM HEPES buffer at pH 8.0. The reaction was conducted by shaking the tubes at 500 rpm for 2 min at 37 °C and quenching the reaction with 6 M HCl. The assay for other metal ions included mixing 50 μM "apo-ADO" with 50 μM metal ions. The results for Fe-ADO were normalized to 50 μM for comparison.

OXYGEN CONSUMPTION ASSAY

The oxygen consumption of ADO reaction was recorded using Oxygraph (Hansatech Pentney, Norfolk, England). The instrument was calibrated using sodium dithionite (DT) solution to establish a zero O_2 level in the reaction chamber. The assay was conducted by adding 50 μM ADO protein in an air-saturated 50 mM HEPES buffer at pH 8. After baseline flatting, 1 mM 2-AET was added to start the reaction. The change of oxygen concentration within 10 min was recorded.

ELECTRON PARAMAGNETIC RESONANCE (EPR) SPECTROSCOPY

A stock solution of cysteamine (1.0 M) or RGS5 peptide (300 mM) was prepared in an anaerobic chamber and added to the enzyme to the final concentration under anaerobic conditions. An equal volume of O_2-saturated 50 mM Tris-HCl, 50 mM NaCl (pH 7.6) buffer was added to anaerobic Co-ADO with 2-AET or RGS5 before being frozen at various intervals. The samples were transferred to quartz EPR tubes and slowly frozen in liquid ethane or nitrogen. EPR spectra were recorded on a Bruker E560 X-band spectrometer equipped with a cryogen-free 4 K temperature system with an SHQE high-Q resonator at 100 kHz modulation frequency, 0.6 mT modulation amplitude, and an average of four scans for each spectrum. The full-range scan was conducted at 3.17 mW microwave power at 30 K. Power saturation experiments for the LS species were performed using microwave power range from 0.0002 to 50.23 mW at 10 K, 30 K, and 50 K. LS-range scan was performed at 0.2 mW microwave power at 50 K. The data analysis of the relation properties followed previously published procedures.[6] The simulations of field-swept CW EPR spectra of frozen solutions were performed using the function pepper from the computational package of EasySpin, which is based on MatLab, a commercial technical computation software.

TRANSIENT-STATE KINETICS ANALYSIS

Stopped-flow experiments were performed at 22 °C, pH 7.6, and investigated at multiple (PDA) wavelengths using Applied Photophysics SX20 Stopped-Flow UV-vis spectrophotometer. The PDA data were analyzed to identify specific single wavelengths for monitoring the formation and decay of intermediates. Representative time courses were fitted to single or double exponential expressions to obtain characteristic observed rate constant (k_{obs}) using the SX Pro-Data Viewer analysis software provided by Applied Photophysics. All concentrations mentioned here were the ones after mixing. Formation of [Co-ADO(2-AET)-O_2] was carried out in a conventional mixing mode with 50 μM enzyme in 50 mM Tris, 50 mM NaCl (pH 7.6) containing 25 μM 2-AET and an equal volume of O_2 saturated 50 mM Tris, 50 mM NaCl (pH 7.6) buffer. Formation and decay of the ternary complex of [Co-ADO(2-AET)-O_2] was monitored at a wavelength of 316 nm.

CRYSTALLIZATION, DATA COLLECTION, MODEL BUILDING, AND REFINEMENT.

Co-ADO was concentrated to 30 mg/ml and mixed at 1:1 (v/v) with a crystallization buffer of 0.1 M BisTris-HCl (pH 5.5), 0.2 M $(NH_4)_2SO_4$, and 20% (w/v) PEG3350 using the hanging drop, vapor-diffusion method at 289 K. Microcrystals formed after 1-2 days and grew to an optimal size suitable for X-ray diffraction after one week. The crystallization of Fe-ADO was conducted in a Coy gloveless anaerobic chamber. Crystals were cryoprotected with crystallization buffer containing an additional 20% (v/v) glycerol and then flash-cooled in liquid nitrogen. Crystallographic data were acquired at 100 K temperature at Stanford Synchrotron Radiation Lightsource beamline BL 9-2 and the Advanced Photon Sources (Argonne National Laboratory, Argonne, IL) beamline 19BM. All X-ray diffraction intensity data were integrated, scaled, and merged using HKL3000.[7] Molecular replacement was performed with Phenix[8] using the crystal structure of Ni-hADO as a starting model (Protein Data Bank entry 7REI).[1] The final model was manually adjusted and refined with Coot[9] and Phenix. Ramachandran statistics were analyzed using MolProbity. All the phi and psi angles were located in the preferred and allowed regions without any outliers. We generated all the molecular model figures using PyMOL (W.L. DeLano, The PyMOL Molecular Graphics System version 1.8.6.0. Schrödinger LLC, http://www.pymol.org/; 2002). The structural data was deposited to the PDB databank with entry codes 8UAN and 8U9J.

Table S1. The S–O bond length in the crystal structures of Fe^{2+}-bound persulfenate intermediate[11-12]

PDB entry Resolution (Å) (pH during crystallization)	3ELN[13] 1.42 (5.6)	4IER[14] 1.45 (5.5)	4IES[15] 1.40 (6.2)	4IET[16] 1.40 (6.8)	4IEU[17] 1.25 (7.0)	4IEY[18] 1.63 (7.0)
S–O bond (proximal O which is near the iron) (Å)	1.7	1.7	1.7	1.7	1.7	1.7
S…O distance (distal O from the iron ion) (Å)	2.6	2.9	3.2	2.9	2.9	2.8

Table S2. Iron ion content and k_{obs} value of Fe-ADO and Co-ADO obtained from an M9 minimum medium[a]

Samples[b]	A_{562}	Concentration of iron	Percentage of iron in protein	k_{obs} calculated by enzyme concentration (min^{-1})	k_{obs} calculated by iron concentration (min^{-1})
Fe-ADO (19.0 μM)	0.295 ± 0.002	10.97 μM	57.73%	30.6 ± 0.3	53.00
Co-ADO (114 μM)[c]	0.050 ± 0.003	1.97 μM	1.73%	2.25 ± 0.04	130.06[d]
"apo-ADO" (125 μM)	0.040 ± 0.007	1.62 μM	1.30%	0.0815 ± 0.002	6.27

[a] The details for determining iron concentration have been described elsewhere.[4]

[b] Fe-ADO and Co-ADO are as-purified proteins using an M9 minimum medium. Reactivities were determined using the HPLC assay.

[c] The EPR signal intensities were obtained by double integration after baseline correction. The quantitation was carried out by comparing to a Cu(II)-EDTA standard and presented as a percentage of the corresponding protein concentration of the samples.

[d] The k_{obs} value of 130.06 min^{-1} calculated solely based on the iron content in Co-ADO is more than the value of 53.00 min^{-1} in Fe-ADO, indicating the contribution form Co(II) in Co-ADO.

Table S3. k_{obs} value of "apo-ADO" with different metal ions

Sample name	"apo-ADO"	+ Mn^{2+}	+ Fe^{2+}	+ Co^{2+}	+ Ni^{2+}	+ Cu^{2+}
k_{obs} (min^{-1}) in air saturated buffer[a]	0.0766 ± 0.0021	0.143 ± 0.012	26.4 ± 1.1	1.45 ± 0.04	0.258 ± 0.004	0.0685 ± 0.0191
Normalization	0.29	0.54	100.00	5.50	0.98	0.26
k_{obs} (min^{-1}) in O_2 saturated buffer	0.207 ± 0.013	0.167 ± 0.020	34.3 ± 3.2	1.50 ± 0.01	0.417 ± 0.010	0.00172 ± 0.01033
Normalization	0.60	0.49	100.00	4.38	1.22	0.01
The ratio of reactivity in O_2/air saturated buffer	2.70	1.17	1.30	1.03	1.62	0.03

[a] The Co(II)-ADO exhibited a k_{obs} value approximately 18.9 ± 0.7-fold higher than that of "apo-ADO," which contains trace iron, while Ni(II)-ADO showed a 3.37 ± 0.11-fold increase. The error range was calculated using the Error propagation calculator available on the website (https://www.eoas.ubc.ca/courses/eosc252/error-propagation-calculator-fj.htm).

Table S4. X-ray crystallographic data collection and refinement statistics

	Co-ADO-Se edge	**Co-ADO-Co edge**	**Fe-ADO-Se edge**
Data Collection	SSRL	SSRL	SBC
Wavelength (Å)	0.97946	1.60471	0.97919
Space group	$C222_1$	$C222_1$	$C2$
Cell dimensions			
a, b, c (Å)	54.9, 95.9, 118.2	55.3, 95.7, 118.8	117.9, 55.2, 97.3
α, β, γ (°)	90, 90, 90	90, 90, 90	90, 114, 90
Resolution (Å)[a]	50.00 – 1.99	50.00 – 2.43	50.00 – 2.01
	(2.02 – 1.99)[a]	(2.47 – 2.43)	(2.04 – 2.01)
Total reflection	141914	251358	157446
Unique reflection	21821	11974	36519
Redundancy	6.5 (6.1)	21.0 (8.8)	4.3 (2.8)
R_{sym} or R_{merge} (%)	16.3 (48.7)	33.6 (157.9)	23.1 (92.3)
I/σI	36.0 (1.8)	14.1 (1.14)	7.9 (1.02)
Completeness (%)	99.7 (98.0)	99.6 (97.2)	96.7 (82.2)
$CC_{1/2}$	0.96 (0.92)	0.90 (0.38)	0.98 (0.66)
Refinement			
Resolution (Å)	47.62 – 1.99		46.84 – 2.02
No. reflections	2217		1885
R_{work}/R_{free} (%)	19.81 / 23.54		20.82 / 25.88
No. Atoms / *B*-factors (Å^2)			
Protein	1888 / 47.5		1912 / 31.8 (A)
Co/Fe	1 / 34.8		1 / 21.5 (A)
Glycerol	24 / 51.5		24 / 41.3
Sulfate	N / A		10 / 57.3
Water	80 / 47.0		281 / 38.1
r.m.s. deviations			
Bond lengths (Å)	0.008		0.008
Bond angles (°)	0.989		1.000
Ramachandran[b]			
Favored (%)	99.13		98.09
Allowed (%)	0.87		1.91
Outlier (%)	0.00		0.00
PDB Code	**8UAN**		**8U9J**

[a] Values in parentheses are for the highest-resolution shell.

[b] Ramachandran statistics were analyzed using MolProbity. Lovell, S. C.; Davis, I. W.; Arendall, W. B., 3rd; de Bakker, P. I.; Word, J. M.; Prisant, M. G.; Richardson, J. S.; Richardson, D. C., Structure validation by C_α geometry: phi, psi and C_β deviation. Proteins 2003, 50(3), 437-50.

Table S5. Comparison of the EPR parameters for Co-ADO complexes and [Co(II)-HPCD(4NC)O_2]

Sample	*S*	*g* value (g_x, g_y, g_z)	*A* (^{59}Co)
Co(II)-ADO	3/2	2.63, 4.25, 5.26	N/A
[Co(II)-ADO(2-AET)]	3/2	2.25, 4.00, 5.71	210 MHz (A_z)
[Co(II)-ADO(RGS5)]	3/2	2.25, 4.00, 5.71	210 MHz (A_z)
[Co(II)-ADO(2-AET)O_2]	1/2	2.00, 2.02, 2.08	67 MHz (A_z)
[Co(II)-ADO(RGS5)O_2]	1/2	2.00, 2.02, 2.08	67 MHz (A_z)
[Co(II)-HPCD(4NC)O_2][a]	1/2	1.99, 2.02, 2.10	67 MHz (A_z)

[a] Fielding, A. J.; Lipscomb, J. D.; Que, L., Jr., Characterization of an O_2 adduct of an active cobalt-substituted extradiol-cleaving catechol dioxygenase. *J. Am. Chem. Soc*. 2012, 134 (2), 796-799.

Table S6. EPR relaxation parameters of power saturation experiments performed on the LS ternary complex

Parameters	10 K	30 K	50 K
$P_{1/2}$ (mW)	0.0181 ± 0.0066	0.319 ± 0.073	2.40 ± 0.45
b value	1.04 ± 0.05	0.954 ± 0.051	1.19 ± 0.08

Table S7. Best fit parameters for X-band EPR spectrum of the ternary complex

Experiment		***S***	***g* value (g_z, g_y, g_x)**	***A* (^{59}Co) MHz (A_z)**
[Co(II)-ADO(2-AET)O_2]		1/2	2.08, 2.02, 2.00	67
Simulation	***I***	***S***	***g* value (g_z, g_y, g_x)**	***A* (^{59}Co) MHz (A_z, A_y, A_x)**
Simulated species	7/2	1/2	2.076, 2.012, 2.001	67, 15, 38

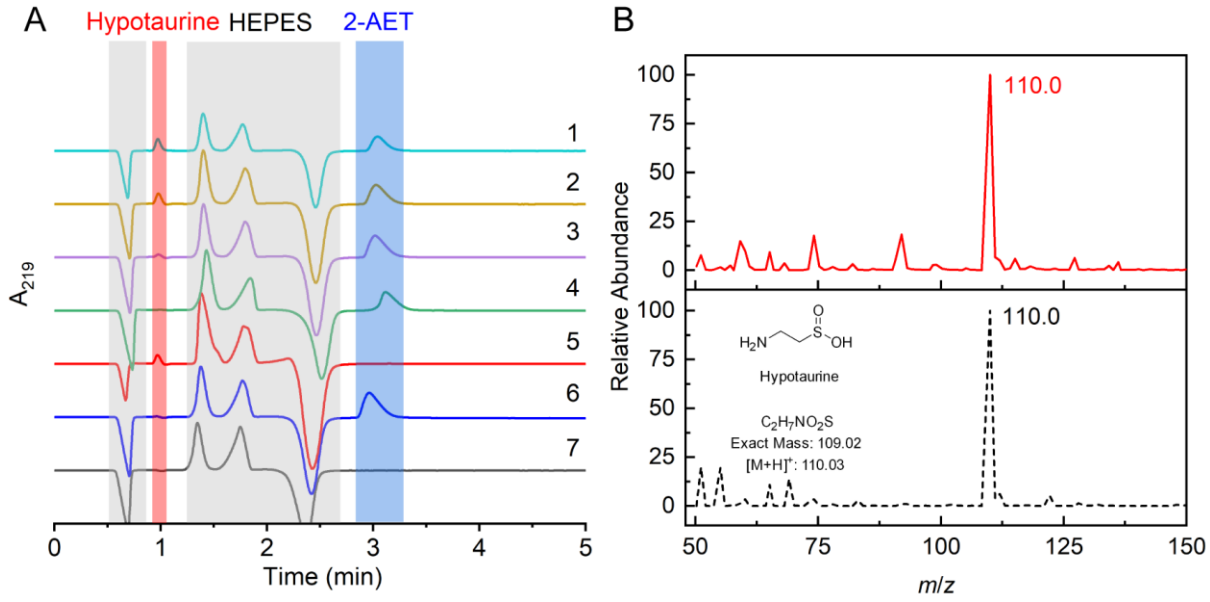

Figure S1. Catalytic activity of human ADO reconstituted from metal-depleted protein by HPLC-MS. (**A**) HPLC elution profiles of the reaction and controls in 50 mM HEPES buffer under aerobic conditions**:** (1) 5 μM metal-depleted "apo-ADO" + Fe(II) + 10 mM 2-AET; (2) 50 μM metal-depleted "apo-ADO" + Co(II) + 10 mM 2-AET; (3) 50 μM metal-depleted "apo-ADO" + 10 mM 2-AET; (4) 50 μM Co(II) + 10 mM 2-AET; (5) 250 μM authentic hypotaurine from a commercial source; (6) 10 mM 2-AET; and (7) 50 mM HEPES buffer, pH 8. The negative peaks in the HPLC elution profiles emerged due to the difference between HEPES buffer in the samples and the HPLC solvent. (**B**) Mass spectrum of the reaction product from reaction 2 (red line) and comparison with an authentic hypotaurine standard from a commercial source (black dash line). The peak with *m*/*z* at 110.0 indicates the presence of hypotaurine. These data demonstrate the dioxygenase catalytic activity of Co(II)-reconstituted ADO towards cysteamine. Similarly, Ni-ADO also shows dioxygenase activity during development of the HPLC-MS assay method,[4] albeit with a smaller activity than Co-ADO's.

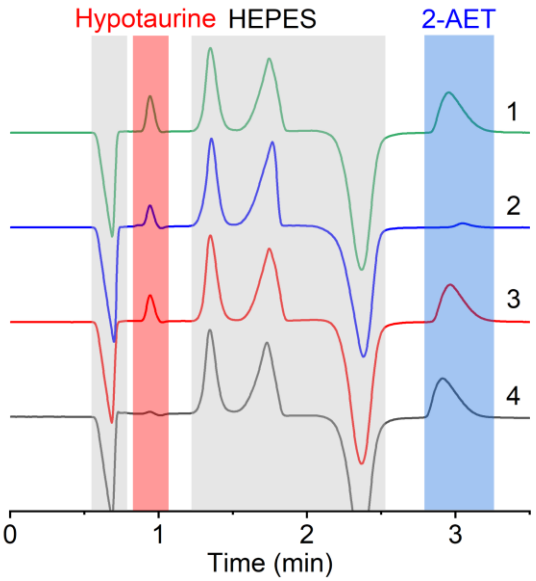

Figure S2. Catalytic activity of metal-reconstituted ADO with protein obtained from an M9 minimum medium. HPLC profiles: (1) 5 μM Fe(II)-reconstituted protein with apo-ADO from M9 minimum medium and 10 mM 2-AET reacted at 37 °C for 2 min under aerobic conditions; (2) 50 μM Co-reconstituted protein with apo-ADO from M9 minimum medium and 1 mM 2-AET reacted at 22 °C for 2 min under aerobic conditions (this lower temperature reaction condition was the same as the oxygen consumption assay in **Figure 3A** in the main text); (3) 50 μM-reconstituted protein with apo-ADO from M9 minimum medium and 10 mM 2-AET reacted at 37 °C for 2 min under aerobic conditions; and (4) 50 μM as-isolated apo-ADO from M9 minimum medium (without metal reconstitution) and 10 mM 2-AET reacted at 37 °C for 2 min under aerobic conditions. The k_{obs} value for Co(II)-reconstituted ADO in sample (2) was 1.48 ± 0.03 min^{-1}, calculated from peak area integration, which is consistent with the oxygen consumption rate (1.44 min^{-1}) shown in **Figure 3A** in the main text**.**

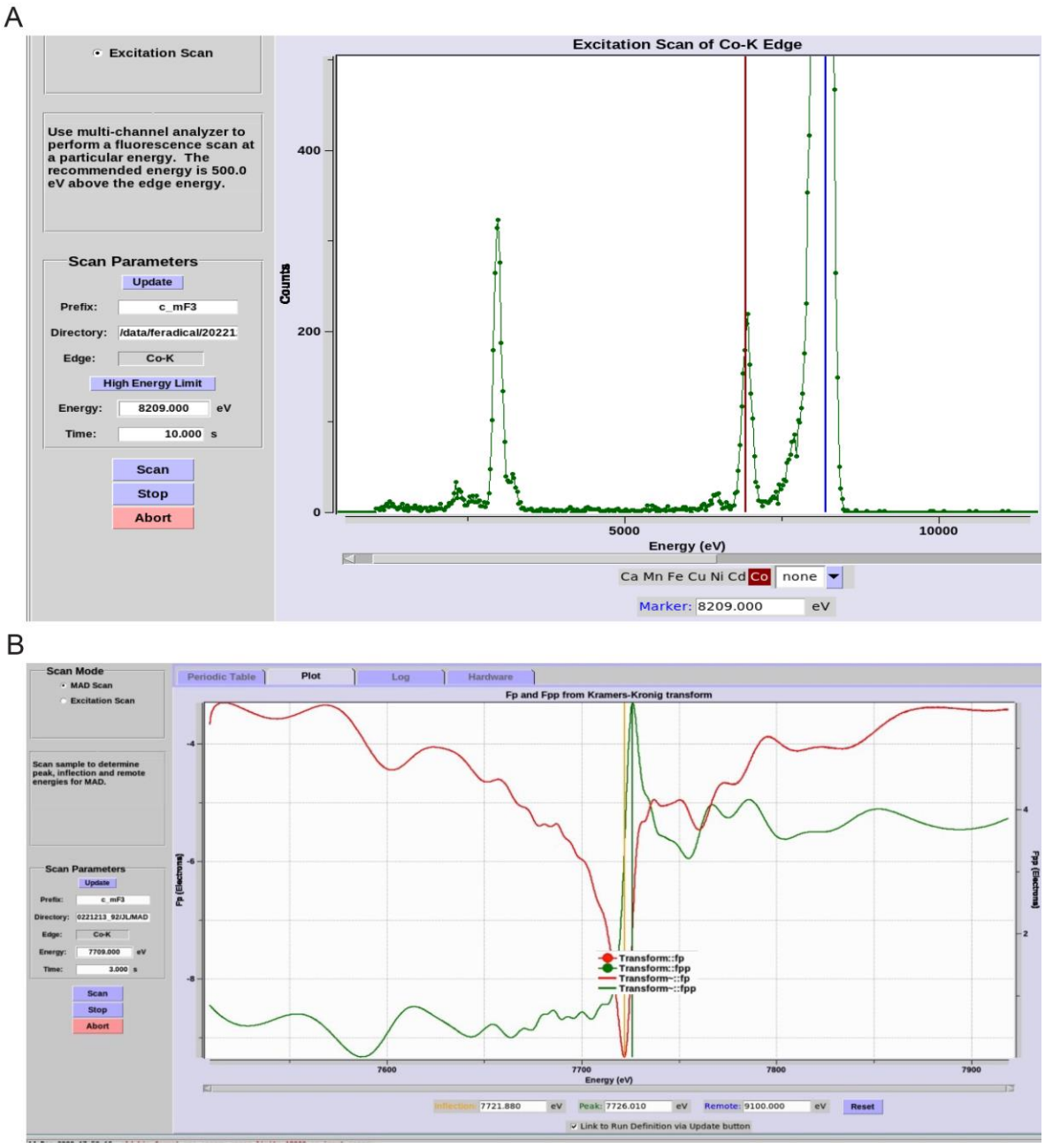

Figure S3. The MAD scan (A) and excitation scan (B) of Co-K edge for Co-ADO crystal. The wavelength used in Co-K edge MAD scan is 1.60471 Å.

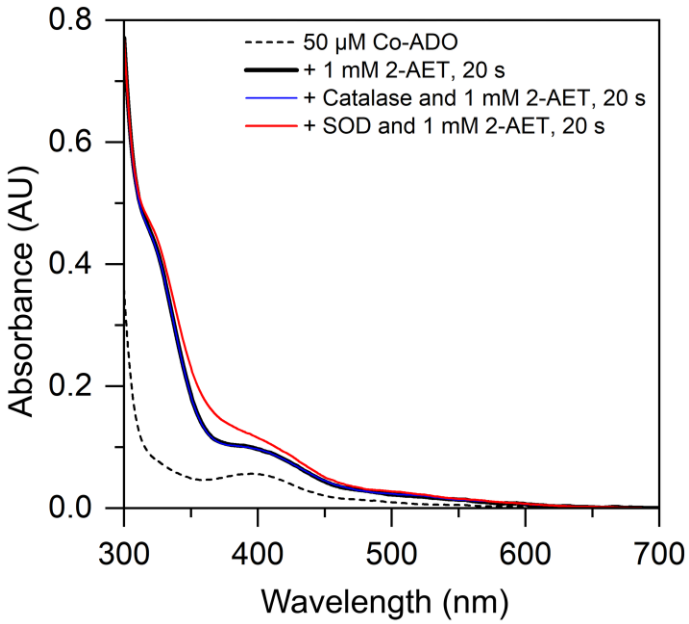

Figure S4. Optical spectral change of Co-ADO incubated with 2-AET and in the presence of catalase or SOD enzymes. The addition of 60 units (as defined by the manufacturer) per mL of catalase (blue) had nearly no influence on the reaction. The addition of 500 units per mL of superoxide dismutase (SOD) (red) had minor influence on the reaction.

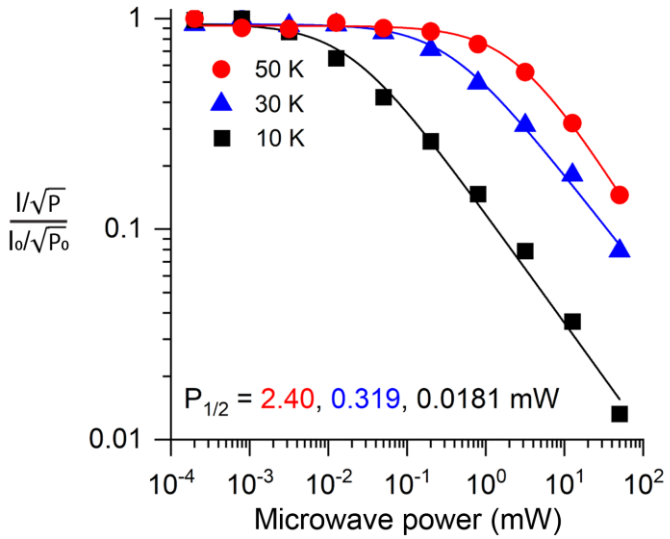

Figure S5. EPR microwave power saturation experiments were performed on the LS species at 10 (black), 30 (blue), and 50 K (red). $P_{1/2}$ values were calculated by fitting plot of signal intensity/square root power ($I/P^{1/2}$) as a function of microwave power with hyperbolic equation. The condition of 0.2 mW and 50 K was chosen for the data collection. The parameters can be found in Table S6. The dominant LS signal at 0.0002 mW follows Curie Law behavior up to 50 K, suggesting it did not originate from a spin-coupled species.

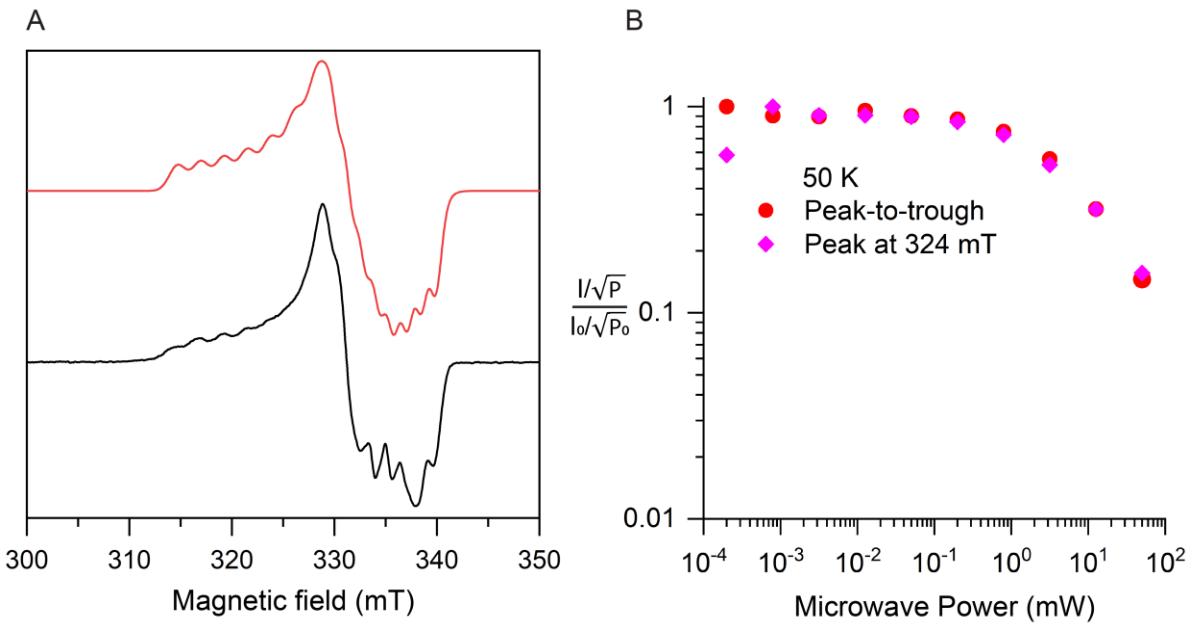

Figure S6. Simulations of the EPR spectrum of the ternary complex. (**A**) X-band EPR spectrum of the ternary complex (black trace) and the best simulated spectrum (red trace). Simulation parameters can be found in Table S7. The best fit of the data leads to an intensive signal characterized by a somewhat rhombic g-tensor (g_z = 2.076, g_y = 2.012, g_x = 2.001), with an anisotropic hyperfine coupling to the $I = 7/2$ nucleus of ^{59}Co (A_z = 67, A_y = 15, A_x = 38 MHz). An end-on Co(III)-superoxo species, reported by Fiedler and co-workers,[11] exhibiting an very similar electronic spectrum as well as comparable EPR spectrum. The g_z and g_y region can be fit well, while the g_x region is a little offset due to the not-well resolved hyperfine splitting lines in the g_x region, which were also observed in Co-HPCD(4NC)-superoxo adduct.[4] (**B**) The two signal amplitudes from peak to trough and at the peak of 324 mT exhibit almost the same relaxation behavior at 50 K, supporting the presence of a single compound in the ternary complex.

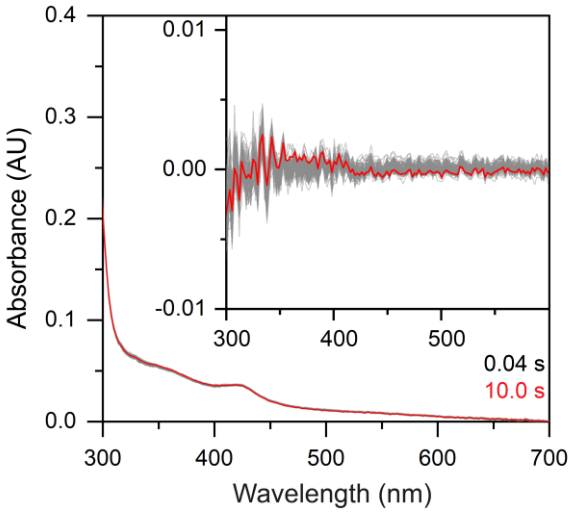

Figure S7. Optical spectral changes of anaerobic apo-ADO with 2-AET upon mixing with O_2. The time scale is from 0.04 (black) to 10 s (red), and the traces between were labeled in grey. The concentration of "apo-ADO" and 2-AET is 30 μM and 0.5 mM, respectively.

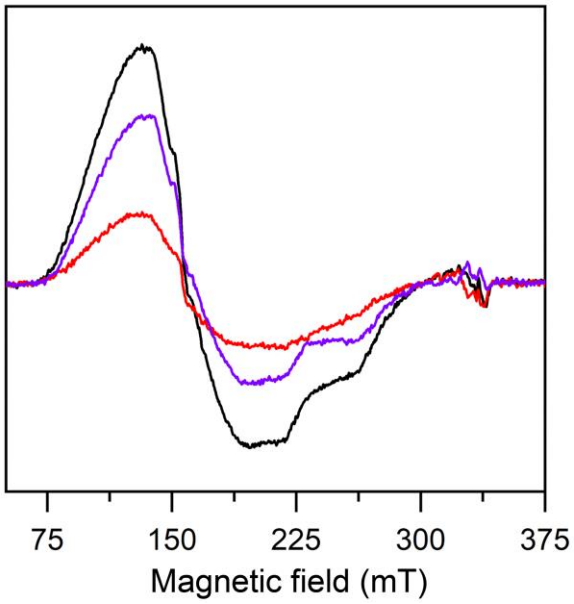

Figure S8. EPR spectral changes of aerobic Co-ADO (black) incubated with 2-AET overnight (red). The concentration of Co-ADO and 2-AET is 200 μM and 20 mM, respectively. Data were collected at 3.17 mW and 30 K. The purple trace shows the difference spectrum. These results indicate that the slower substrate oxidation by the putative Co(III)-superoxo during multiple turnover conditions may trigger a non-productive side route and impact the enzyme's ability to fully return to the resting state.

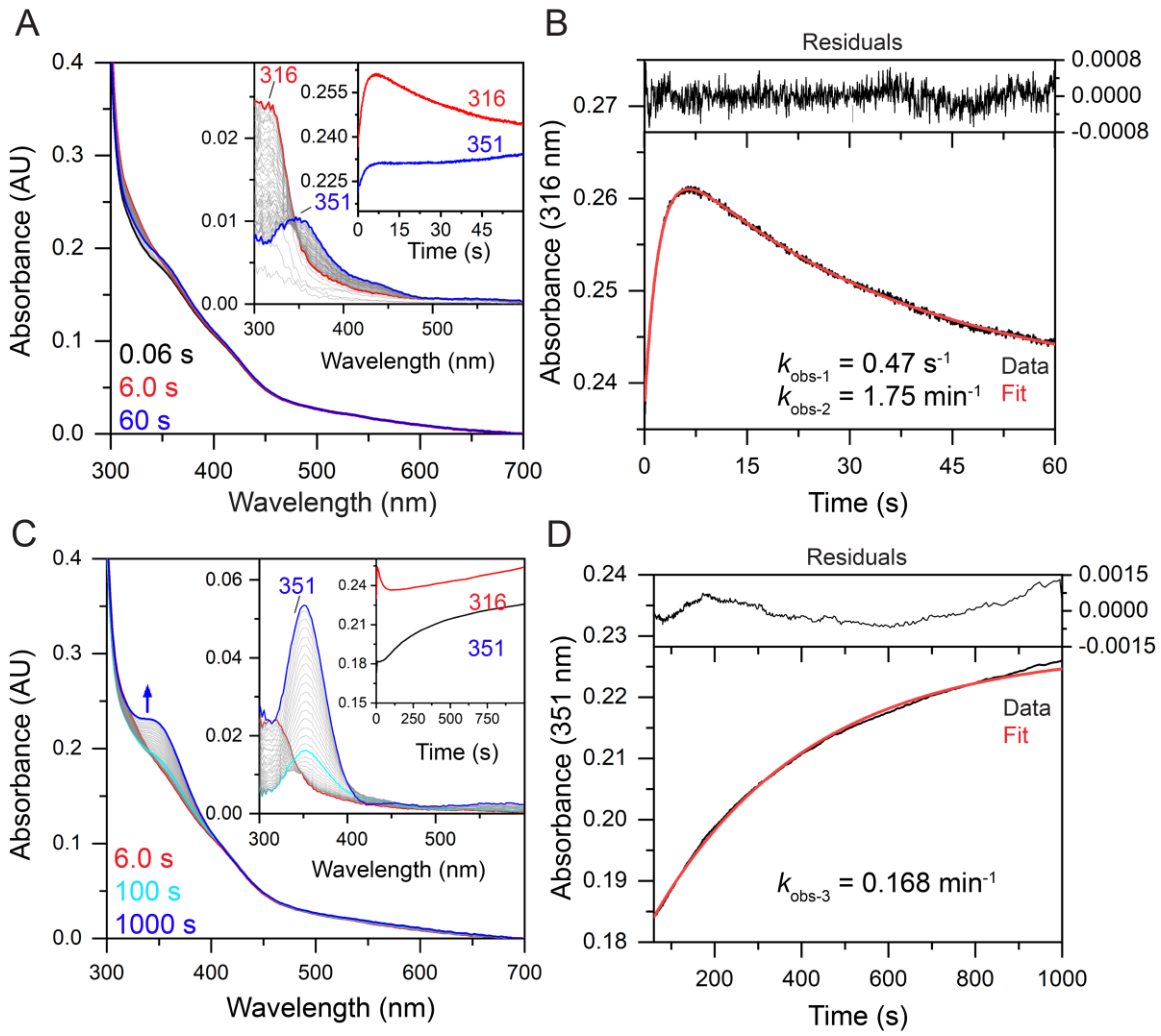

Figure S9. Near "single turn-over" kinetic assay for Co(II)-ADO with 2-AET upon mixing with O_2 and the corresponding data fitting. (**A**) Optical spectral changes of anaerobic Co(II)-ADO (50 μM) with 25 μM 2-AET upon adding O_2-saturated buffer from 0.06 s (black) to 6 s (red)and 60 s (blue). (**B**) Representative time courses at 316 nm (black), superimposed fits (red), and residuals from 0.16 to 60 s. A double-exponential expression was employed for data fitting. The estimated $t_{1/2}$ value of the ternary complex was 24 s, calculated using the rate constant (k_{obs-2}) of 1.75 min^{-1}. (**C**) Optical spectral changes of anaerobic Co(II)-ADO (50 μM) with 25 μM 2-AET upon adding O_2-saturated buffer from 6 s (red) to 100 s (cyan) and 1,000 s (blue). (**D**) Representative time courses at 351 nm (black), superimposed fits (red), and residuals from 6 to 1,000 s. A single-exponential expression was employed for data fitting. The observed 351 nm species in the near 'single turn-over' kinetic assay is tentatively assigned to a product or byproduct bound to Co-ADO. The nature of this species requires further investigation in the future.

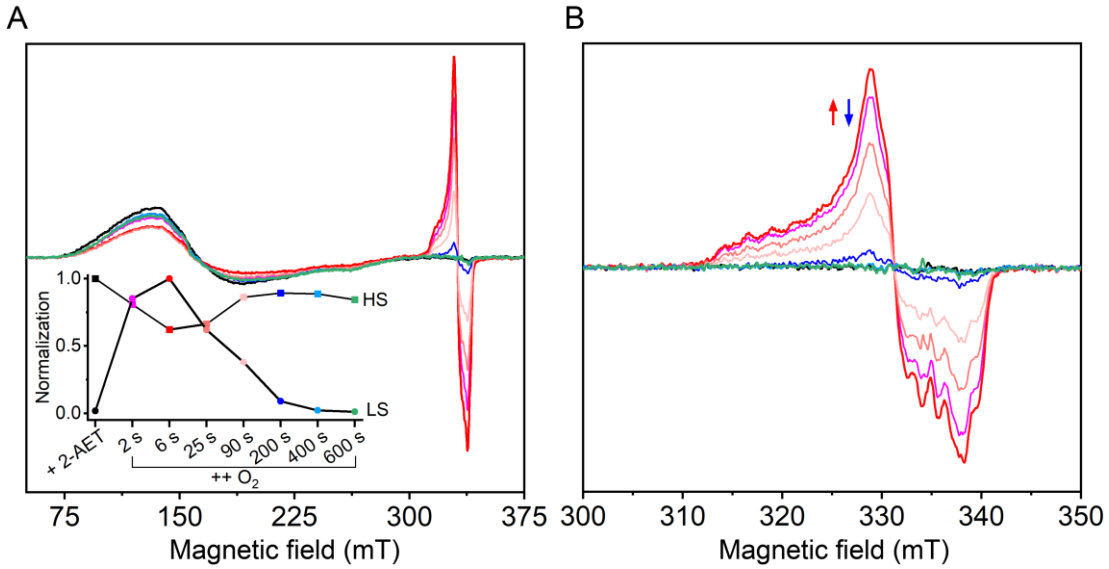

Figure S10. EPR spectral changes of anaerobic Co-ADO (100 μM) with 2-AET (50 μM) upon O_2 addition. (**A**) Full scan EPR spectral data collected at 3.17 mW and 30 K. The spectrum of resting Co-ADO is labeled in black trace; The spectra at 2, 6, 25, 90, 200, 400, and 600 s are labeled in magenta, red, light red, pale red, blue, light blue, and green, respectively. The inset shows time-dependent intensity variations, specifically highlighting the peak to trough changes of the HS (A) and LS (B) species. (**B**) Narrow scan for the LS species (0.2 mW at 50 K temperature).

References

1. (a) Wang, Y.; Shin, I.; Li, J.; Liu, A. Crystal structure of human cysteamine dioxygenase provides a structural rationale for its function as an oxygen sensor. *J. Biol. Chem.* **2021**, *297*, 101176. (b) Wang, Y.; Davis, I.; Yang, Y.; Chen, Y.; Naik, S.G.; Griffith, W.P.; Liu, A. Characterization of the non-heme iron center of cysteamine dioxygenase and its interaction with substrates. *J. Biol. Chem*. **2020**, 295, 11789-11802. (c) Wang, Y.; Griffith, W.P.; Li, J.; Koto, T.; Wherritt, D.; Fritz, E.; Liu, A.; Cofactor biogenesis in cysteamine dioxygenase: C-F bond cleavage with genetically incorporated unnatural tyrosine. *Angew. Chem. Int. Ed*. **2018**, *57*, 8149-8153.
2. Ren, D.; Lee, Y. H.; Wang, S. A.; Liu, H. W. Characterization of the oxazinomycin biosynthetic pathway revealing the key role of a nonheme iron-dependent mono-oxygenase. *J. Am. Chem. Soc.* **2022**, *144*, 10968-10977.
3. Tchesnokov, E. P.; Wilbanks, S. M.; Jameson, G. N. L. A strongly bound high-spin iron(II) coordinates cysteine and homocysteine in cysteine dioxygenase. *Biochemistry* **2012**, *51*, 257-264.
4. Duan, R.; Li, J.; Liu, A. Unveiling the mechanism of cysteamine dioxygenase: A combined HPLC-MS assay and metal-substitution approach. *Methods Enzymol.* **2024**, *703*, 29, AID 2589.
5. Chen, Y. The structure and function study of three metalloenzymes that utilize three histidines as metal ligands, Dissertation. 2013, Georgia State University, https://scholarworks.gsu.edu/chemistry_diss/86.
6. Liu, A.; Pötsch, S.; Davydov, A.; Barra, A. L.; Rubin, H.; Gräslund, A. The tyrosyl free radical of recombinant ribonucleotide reductase from *Mycobacterium tuberculosis* is located in a rigid hydrophobic pocket. *Biochemistry* **1998**, *37*, 16369-16377.
7. Otwinowski, Z.; Minor, W. Processing of X-ray diffraction data collected in oscillation mode. *Methods Enzymol.* **1997**, *276*, 307-326.
8. Adams, P. D.; Afonine, P. V.; Bunkóczi, G.; Chen, V. B.; Davis, I. W.; Echols, N.; Headd, J. J.; Hung, L. W.; Kapral, G. J.; Grosse-Kunstleve, R. W.; McCoy, A. J.; Moriarty, N. W.; Oeffner, R.; Read, R. J.; Richardson, D. C.; Richardson, J. S.; Terwilliger, T. C.; Zwart, P. H. PHENIX: a comprehensive Python-based system for macromolecular structure solution. *Acta Crystallogr D Biol Crystallogr.* **2010**, *66*, 213-221.
9. Emsley, P.; Cowtan, K. Coot: model-building tools for molecular graphics. *Acta Crystallogr D Biol Crystallogr.* **2004**, *60*, 2126-2132.
10. Fischer, A. A.; Lindeman, S. V.; Fiedler, A. T. Spectroscopic and computational studies of reversible O_2 binding by a cobalt complex of relevance to cysteine dioxygenase. *Dalton Trans.* **2017**, *46*, 13229-13241.
11. Simmons, C. R.; Krishnamoorthy, K.; Granett, S. L.; Schuller, D. J.; Dominy, J. E., Jr.; Begley, T. P.; Stipanuk, M. H.; Karplus, P. A. A putative Fe^{2+}-bound persulfenate intermediate in cysteine dioxygenase. *Biochemistry* **2008**, *47*, 11390-11392.
12. Driggers, C. M.; Cooley, R. B.; Sankaran, B.; Hirschberger, L. L.; Stipanuk, M. H.; Karplus, P. A. Cysteine dioxygenase structures from pH 4 to 9: consistent cys-persulfenate formation at intermediate pH and a Cys-bound enzyme at higher pH. *J. Mol. Biol.* **2013**, *425*, 3121-3136.
13. Simmons, C. R.; Stipanuk, M. H.; Karplus, P. A. PDB entry 3ELN: A putative Fe^{2+}-bound persulfenate intermediate in cysteine dioxygenase *RCSB PDB Database* **2008**, https://doi.org/10.2210/pdb2213ELN/pdb.
14. Driggers, C. M.; Cooley, R. B.; Karplus, P. A. PDB entry 4IER: Cys-persulfenate bound cysteine dioxygenase at pH 5.5 in the presence of Cys. *RCSB PDB Database* **2012**, https://doi.org/10.2210/pdb2214IER/pdb.
15. Driggers, C. M.; Cooley, R. B.; Sankaran, B.; Karplus, P. A. PDB entry 4IES: Cys-persulfenate bound cysteine dioxygenase at pH 6.2 in the presence of Cys. *RCSB PDB Database* **2012**, https://doi.org/10.2210/pdb2214IES/pdb.
16. Driggers, C. M.; Cooley, R. B.; Karplus, P. A. PDB entry 4IET: Cys-persulfenate bound cysteine dioxygenase at pH 6.8 in the presence of Cys. *RCSB PDB Database* **2012**, https://doi.org/10.2210/pdb2214IET/pdb.
17. Driggers, C. M.; Cooley, R. B.; Karplus, P. A. PDB entry 4IEU: Cys-persulfenate bound cysteine dioxygenase at pH 7.0 in the presence of Cys. *RCSB PDB Database* **2012**, https://doi.org/10.2210/pdb2214IEU/pdb.
18. Driggers, C. M.; Cooley, R. B.; Karplus, P. A. PDB entry 4IEY: Cys-persulfenate bound cysteine dioxygenase at pH 7.0 in the presence of Cys, home-source structure. *RCSB PDB Database* **2012**, https://doi.org/10.2210/pdb2214IEY/pdb.